Journal of Catalysis 395 (2021) 46–53

Contents lists available at ScienceDirect

Journal of Catalysis

journal homepage: www.elsevier.com/locate/jcat

N_8 stabilized single-atom Pd for highly selective hydrogenation of acetylene

Maocong Hu [a,b], Zhiyi Wu [a], Zhenhua Yao [a,b], Joshua Young [a], Langli Luo [c], Yingge Du [c], Chongmin Wang [c], Zafar Iqbal [a], Xianqin Wang [a,*]

[a] Department of Chemical and Materials Engineering, New Jersey Institute of Technology, Newark, NJ 07102, USA
[b] Hubei Key Laboratory of Industrial Fume and Dust Pollution Control, and Key Laboratory of Optoelectronic Chemical Materials and Devices of Ministry of Education, School of Chemical and Environmental Engineering, Jianghan University, Wuhan 430056, China[1]
[c] Pacific Northwest National Laboratory, Richland, WA 99352, USA

ARTICLE INFO

Article history:
Received 30 September 2020
Revised 4 December 2020
Accepted 14 December 2020

Keywords:
Single-atom catalyst
Selective hydrogenation of acetylene
Polynitrogen
Cyclic voltammetry
Density functional theory

ABSTRACT

Single-atom catalysts show a promising future in many reactions even though great challenges still remain such as facile synthesis and long stability. In this work, a single-atom Pd catalyst attached to a designed N_8 Lewis base species (Pd_1-N_8/CNT) is synthesized with cyclic voltammetry (CV) method. The catalyst demonstrates long stability and enhanced C_2H_4 selectivity in selective hydrogenation of acetylene at 40 °C. CV is carried out in a three-electrode setup with PdO/CNT as the working electrode in NaN_3 solution. HAADF-STEM confirms single-atom Pd sites are successfully isolated. XPS measurements and Bader charge calculations indicate N_8 is effectively synthesized on CNT substrate after CV treatment while single-atom Pd is stabilized by attaching to the end N of N_8. Acetylene-temperature programed desorption (C_2H_2-TPD) and density functional theory (DFT) calculations suggest C_2H_2 favors the π bonding on single Pd atom, while H_2 dissociates on the N atom (next to Pd) instead of conventionally on Pd. The synergistic effect favors C_2H_4 formation but prevents full hydrogenation of acetylene to C_2H_6. This work opens up a new perspective to design and synthesize more selective catalysts with isolated single-atom sites.

1. Introduction

Active-site isolation is a promising solution for improving selectivity of hydrogenation reactions such as selective hydrogenation of acetylene, a common method for removing traces of acetylene in ethylene feed streams for ethylene polymerization [1–4]. The basic principle of the isolation is through eliminating the presence of ensembles of active sites on the surface, which is palladium (Pd) ensembles in acetylene case [5,6]. Adding another metal to cover some Pd sites by forming an alloy or Pd intermetallic compounds are two common approaches to eliminate Pd ensemble sites [7–10]. Almost all industrial catalysts for selective hydrogenation of acetylene are alloyed with Ag or Pb as a structural diluent [11]. However, alloys suffer from segregation of Pd to form large Pd particles with time on stream, resulting in limited selectivity and stability [12,13]. Intermetallic compound catalysts require operating at elevated temperatures (200 °C) which restricts wide application [14–16]. Another alternative approach developed in recent years to make active-site isolated catalysts is using single-atom catalysts (SACs) [17–21]. Although SACs have demonstrated attractive performance, great challenges still remain, such as difficulty in scaleup, controllable and facile synthesis of SACs with fine and dense dispersion, and the sacrifice of second noble metal, such as gold or silver [22–24].

Cyclic voltammetry (CV) has become an important and widely used electrochemical process in many areas [25]. Recently, CV is also employed to prepare novel materials including catalysts because of the least requirement of the additives and absence of any interfering products generated, compared to chemical or hydrothermal synthesis methods [26,27]. An N_8^- polynitrogen (PN) phase-based catalyst was successfully synthesized using CV at ambient conditions for the oxygen reduction reaction (ORR). The ORR results showed that lone pairs from PN are very active as an electron donor [28], a novel Lewis base. The intrinsic electron-donor nature of PN suggests it can be an adsorption site for Lewis acid reactants, such as acetylene. Meanwhile, the electronic interactions between Pd and PN may change catalytic property of Pd [29]. Herein, we use the CV process to synthesize a novel

* Corresponding author.
E-mail address: xianqin.wang@njit.edu (X. Wang).
[1] Current address.

https://doi.org/10.1016/j.jcat.2020.12.009
0021-9517/

catalytic system with isolated single-atom Pd sites and novel Lewis base species under ambient conditions for selective hydrogenation of acetylene. The catalyst structure and reaction mechanism were systematically investigated by both advanced experimental techniques and theoretical computations. To the best of our knowledge, there has no previous report on such a method to isolate single-atom site and attach it to designed Lewis base sites for such a reaction. This work opens up a new perspective of synthesizing active-site isolated catalysts.

2. Experimental

2.1. Catalysts preparation

All the materials and chemicals were commercially available and were used without further purification. Round-shaped multi-walled carbon nanotubes (CNT, purchased from Nanolab) sheet was obtained following our previous work [28], Round-shaped 0.8%PdO/CNT sheet was prepared by the reported route [30], using $Pd(NH_3)_4(NO_3)_2$ (Strem 99%) as palladium source and round-shaped CNT sheet as support. To synthesize Pd_1-N_8/CNT catalysts, PdO/CNT sheet was used as the working electrode. CV was carried out using computer-controlled CH Instruments 832C in a three-electrode setup. The PdO/CNT sheet was dipped in 40 mL 0.5–2 M NaN_3 (Aldrich) dissolved in a buffer solution (pH 4.0), which was used as the electrolyte. Pt and Ag/AgCl were used as the counter electrode and standard reference electrode, respectively. The CV scan rate was set to be 1 mV/s and the potential range was set to be between + 0.8 V and −0.8 V. The sample was scanned for 12 CV cycles and then dried overnight in the air. CV was also carried out on PdO/CNT sheet without NaN_3 in the solution to clarify the oxidation peak from N_3^-. The samples were labeled as 0 M, Pd_1-N_8/CNT-0.5 M, Pd_1-N_8/CNT-1 M and Pd_1-N_8/CNT-2 M based on NaN_3 concentration (Table S1). Two references samples were also synthesized. PdO/CNT sheet was dipped in the same kind of electrolyte (1 M NaN_3 inside) without CV scanning and was denoted as 1 M*. The same CV was done with CNT sheet as working electrode and labeled as PN/CNT.

2.2. Catalysts characterization

FTIR was carried out using a Nicolet ThermoElectron FTIR spectrometer combined with a MIRacle ATR platform assembly and a ZnSe plate. Raman spectroscopy was performed with a Thermo Scientific DXR Raman microscope. Atomic resolution high-angle annular dark-field scanning transmission electron microscopy (HAADF-STEM) images were obtained on a FEI Titan STEM/TEM equipped with a probe-corrector. X-ray photoelectron spectroscopy (XPS) measurements were performed with a Kratos Axis Ultra DLD spectrometer using a monochromatic Al Ka X-ray (1486.7 eV) source. The binding energy for all samples was calibrated by the reference C1s binding energy (285.0 eV). The samples were dry dispersed onto a holey carbon film coated copper grid. Elemental analysis of the samples was carried out by Inductively Coupled Plasma Mass Spectrometry ICP-MS (Agilent, 7700X). Temperature-programmed decompositon (TPD) was carried out using a Micromeritics AutoChem II 2920 system. Samples were heated in flowing helium from room temperature to 750 °C at a heating rate of 10 °C/min. The effluent gas was analyzed with an on-line mass spectrometer (QMS 200, Stanford Research Systems). Acetylene-Temperature Programed Desorption (C_2H_2-TPD) was carried out using the same apparatus described previously for TPD test. Catalysts were pre-reduced and exposed to acetylene till the sample was saturated before heated to 750 °C at a heating rate of 10 °C/min in in a 50 mL/min flow of helium. Temperature-programmed oxidation (TPO) was carried out on fresh and used catalysts. Catalyst was maintained in a stream of 10 vol% oxygen and 90 vol% helium with flow rate of 30 mL/min and heating rate 10 °C/min to 500 °C. On-line mass spectrometer (QMS 200, Stanford Research Systems) was used to detect the effluent gas. CO chemisorption was measured by the AutoChem 2920 II (Micromeritics) equipped with a thermal conductivity detector (TCD).

2.3. Computational methods

Density functional theory calculations were performed using the ORCA software package [31]. The geometric optimizations and numerical frequencies were computed using the def2-TZVPP basis set and B3LYP functional [32]. The carbon nanotube was created in a (5,5) armchair configuration with the ends terminated by H atoms, and modelled using the def-SVP basis set; the def2-TZVPP basis set was maintained for PN and Pd in the CNT. All reported energies contain zero point energy corrections. Relaxed surface scans were performed to identify transition states; all transition states were verified by the presence of a single imaginary frequency in the vibrational spectrum. The atomic charges were computed by the Mulliken approach [33].

2.4. Reaction performance testing

The selective hydrogenation of acetylene reactions were performed in a continuous fixed-bed reactor. Catalyst was stabilized on quartz wool which was supported by SiC (40–60 mesh average grain size, Alfar Aesar). ~ 50 mg of catalyst was mixed with 500 mg SiC to minimize temperature gradients. Before reaction, the samples were activated by 10% hydrogen/Argon with a flow rate of 30 mL min^{-1} at 220 °C for 1 h and then cooled to reaction temperature (40 °C). A mixture of acetylene (2%), hydrogen (4%) and ethylene (20%) in a balance of argon with flow rate of 10 mL min^{-1} was passed through the reactor and the products were analyzed with an online gas chromatograph (Agilent, model 6890 with FID) using a HP-PLOT/Q column. C_2H_4 and C_2H_6 were the only gaseous products while no C3 or C4 products were detected by GC/FID. Carbon balance determined from the effluent gas was 100% ± 0.5%. Acetylene conversion X and selectivity toward ethylene $S_{C_2H_4}$ are defined by Eqs. (1) and (2) [34,35], where C_f is the gas concentration in the feed, C_e is the gas concentration in the effluent stream.

$$X = \frac{C_f^{C_2H_2} - C_e^{C_2H_2}}{C_f^{C_2H_2}} \times 100\% \quad (1)$$

$$S_{C_2H_4} = \frac{C_e^{C_2H_4} - C_f^{C_2H_4}}{C_f^{C_2H_2} - C_e^{C_2H_2}} \times 100\% \quad (2)$$

3. Results and discussion

The catalyst preparation with CV process was demonstrated (Fig. S1 and Table S1). There are two peaks detected during the CV process as shown in Figs. 1 and S2. The weak oxidation peak is from azide anion oxidation while the much stronger reduction peak is due to the reduction of PdO to Pd. The oxidation reaction pathway can be denoted as: $N_3^- \rightarrow N_3^* \rightarrow [N\text{-}N\text{-}N]_n$, where the azide ions are irreversibly oxidized to azide radicals which can form long and well-ordered N_8^- polynitrogen (PN) species on the CNT sheets [28]. Fourier-transform infrared (FTIR) and Raman results further confirm the formation of PN (Fig. 2a/b). The characteristic peak at 2100 cm^{-1} from 1 M* (PdO/CNT sheet dipped in 1 M NaN_3 without CV) is the asymmetric stretching mode of azide ion; 2050 cm^{-1}

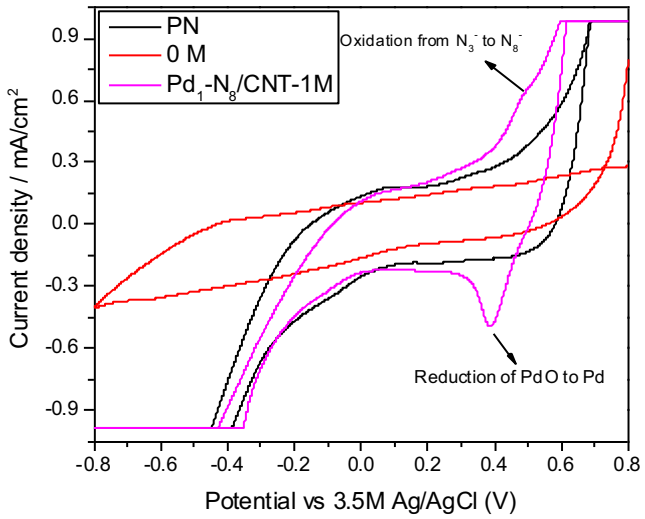

Fig. 1. One typical cycle of CV during the synthesis of isolated single-atom Pd with designed PN over CNT sheet. See Fig. S1 for the whole 12 cycles of stable curves.

from Pd_1-N_8/CNT-1 M (PdO/CNT sheet dipped in 1 M NaN_3 with CV) is the Bu symmetric stretching mode from the C_{2h} structure of N_8 [28] (Fig. 2a). The 1080 cm^{-1} peak from Pd_1-N_8/CNT-1 M, which is not detected from 1 M*, is ascribed to A_G symmetric stretching mode of the C_{2h} structure of N_8 [28](Fig. 2b). The evidence for assigning the reduction peak to the reaction ($PdO + 2H^+ + 2e = Pd + H_2O$) was from theoretical calculation results (Table S2). Corresponding potentials for Pd_1-N_8/CNT-0.5, 1 and 2 M were calculated to be 0.613 V, 0.591 and 0.581 V by the Nernst equation, respectively, based on their pH values and standard potential (0.917 V) of this reaction [36]. After subtracting the potential (0.205 V) from 3.5 mol/L Ag/AgCl (standard reference electrode during CV) [37], the derived potential values (0.408, 0.386 and 0.376 V) are consistent with the experimental findings shown in Fig. 1 (0.410, 0.385 and 0.375 V).

The dispersion and configuration of the Pd sites on the CNT sheet after CV treatment were characterized by atomic resolution high-angle annular dark-field scanning transmission electron microscopy (HAADF-STEM). Compared to the Pd/CNT sample (Pd nanoparticles with non-uniform size of 1–8 nm, Fig. 2c), HAADF-STEM displayed that Pd nanoparticles were barely present on Pd_1-N_8/CNT-1 M while individual Pd atoms randomly disperse on the outer-, intra-, and inter-layers of the nanotubes in the CNT sheet (Fig. 2d). To clarify the completely different morphology of Pd/CNT and Pd_1-N_8/CNT-1 M, ICP-MS was carried out (second column of Table S3). The nominal palladium loading of PdO/CNT sheet was 0.8 wt%. The actual loading was determined to be close to it (0.67 wt%). The slight difference can be attributed to the incom-

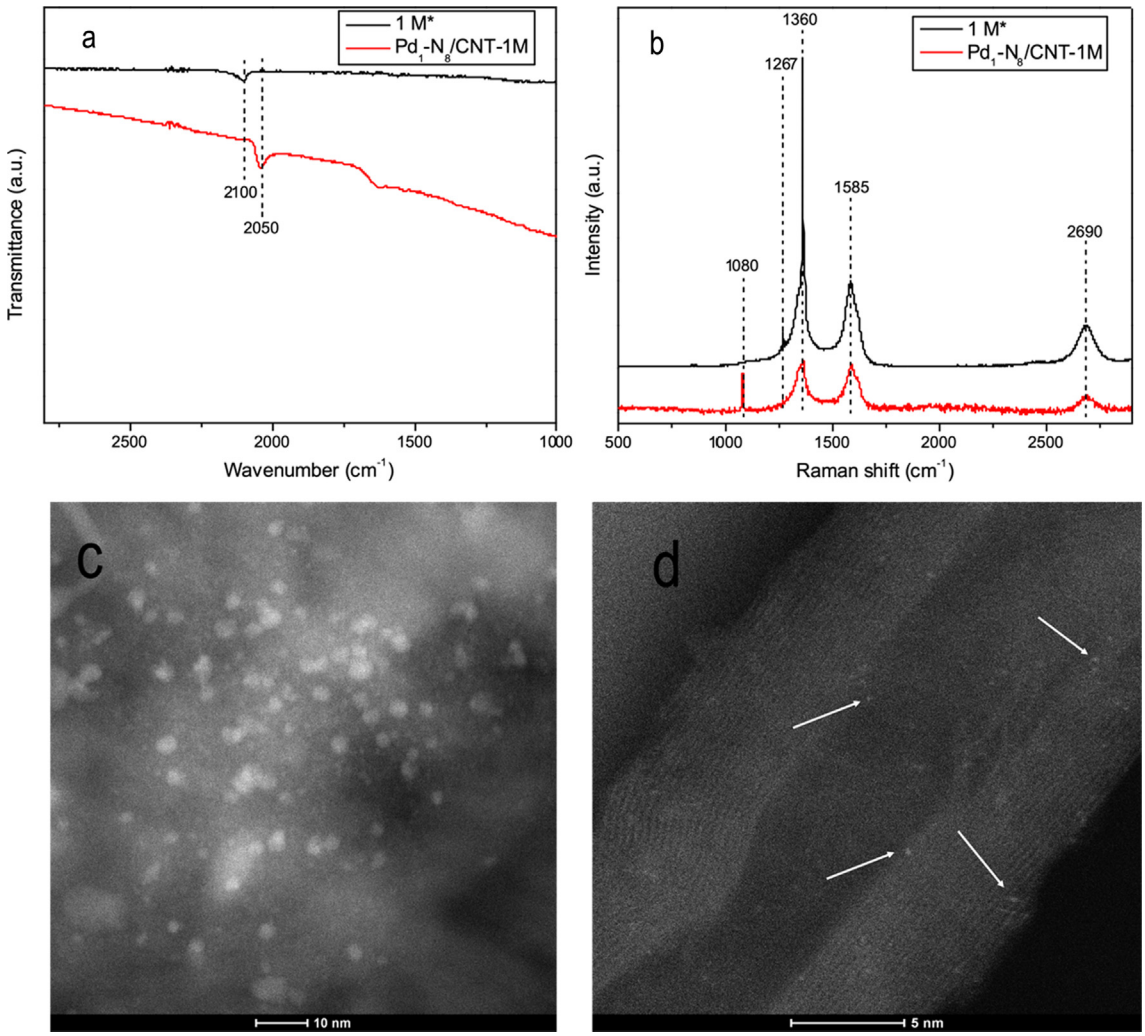

Fig. 2. FTIR (a) and Raman (b) results of 1 M* and Pd_1-N_8/CNT-1 M sample; Representative HAADF-STEM images of nanoparticles of Pd/CNT (c) and single atoms of Pd_1-N_8/CNT-1 M (d), atomically dispersed Pd atoms in image (d) are highlighted by the white arrows, more single-atom images are available in Fig. S3.

plete impregnation during the ethanol vaporization preparation process [30]. After CV treatment in the electrolyte without NaN_3, the Pd loading of 0 M did not change much (0.65 wt%). However, the Pd loading of 1 M* sample (dipped in electrolyte with NaN_3 but without CV) decreased by more than one third (0.41 wt%). These results indicated that azide would facilitate Pd removal as a result of hydrazoic acid formation during NaN_3 dissolution in buffer solution [38]. Interesting results were found on samples with CV treatment in NaN_3 containing electrolyte. The final Pd loadings in all three samples with CV and NaN_3 containing electrolyte are very low (0.00018–0.033 wt%). This extremely low metal loading enables the possible atomic dispersion of Pd on CNT as observed in Fig. 2d. We also calculated the integrated charges that passed through the electrode for the reduction peak in all 12 cycles and compared it with the value from the theoretical derivation (Table S4) based on the assumption that the reduced Pd (metallic Pd) by CV was mostly eliminated. The integrated result from CV (0.557741C) is in a good agreement with the value derived based on ICP-MS measurement (0.558084C). Therefore, it could be concluded only Pd single atoms are left on the CNT support after CV process. The eliminated Pd in the electrolyte can be recovered by a room temperature electron reduction approach [39].

The interactions among the components of Pd_1-N_8/CNT were first investigated by XPS (Figs. 3 and S4). In addition to the peak at 285.0 eV ascribed to C—C bonds from CNT, the C1s spectrum of Pd_1-N_8/CNT-1 M (Fig. 3a) shows a distinct peak at around 285.9 eV, which is absent in Pd/CNT and is different from C-N bond in carbon nitride (with binding energy at 288.1 eV) [40]. Moreover, in consideration of electronegativity order (Pd < C < N), this peak should not be related to any Pd-C interactions. Thus, it's reasonable to attribute it to a C-N_8 structure due to the attachment of N_8 on CNT surface. This unique structure would stabilize the synthesized N_8 as predicted by previous computational results [41]. The Pd $3d_{5/2}$ peak of PdO/CNT located at 338.2 eV (Fig. S4), is from the 2 + valence state of Pd [1]. The Pd $3d_{5/2}$ peaks of Pd_1-N_8/CNT-1 M and Pd_1-N_8/CNT-0.5 M samples systematically shift to higher binding energy 339.1 eV from Pd^{4+} [42]. The higher valence of Pd species on Pd_1-N_8/CNT is likely due to a charge transfer from Pd to N_8, which can be attributed to the high electronegativity of N_8 compared to Pd, through a previously proposed exchange-transfer mechanism [43,44]. It would decrease the electron density of the Pd atoms. The interaction of a Pd atom with N_8 was further investigated by DFT calculations (details are described in DFT section below) (Fig. 3b). The adsorption energy of a single Pd atom on the end of an N_8 chain was determined to be $E_{ads} = -1.03$ eV, indicating this interaction is energetically favorable. Moreover, a Mulliken charge calculation indicates that there is a stabilizing charge transfer of 0.23 *e* from the Pd atom to the PN chain, which is in agreement with experimental XPS measurements. The interaction between Pd and N_8 facilitated the stabilization of single-atom Pd, which was evidenced by HAADF-STEM image in Fig. 2. Furthermore, the electronic effect originating from the Pd-N_8 will change the catalyst reaction performance in selective hydrogenation of acetylene.

Temperature-programmed decomposition was carried out to test the thermal stability of the Pd_1-N_8/CNT catalysts. As shown in Fig. 4a, nitrogen desorbed at 346 °C on dipped Pd/CNT (1 M*) sample, which was attributed to azide decomposition [45]. A higher desorption temperature was observed on samples with CV treatment, indicating that Pd_1-N_8/CNT catalysts are thermally stable [28]. It can be attributed to the stabilizing effect of C-N_8 structure as revealed in the above XPS analysis. Moreover, the stability of three CV treated samples followed the trend of Pd_1-N_8/CNT-0.5 M > Pd_1-N_8/CNT-1 M > Pd_1-N_8/CNT-2 M. During the CV process, synthesized N_8 first deposited on the CNT surface with C-N_8 structure, which led to a relatively stable state (Pd_1-N_8/CNT-0.5 M case). When the azide concentration increased, the formed N_8 amount increased.[11] More layers of N_8 would form on the CNT surface, but only the first layer has C-N_8 interaction (Pd_1-N_8/CNT-1 M and Pd_1-N_8/CNT-2 M case), which resulted in a relatively lower decomposition temperature. The N_8 decomposition temperature on Pd_1-N_8/CNT is slightly lower than that on N_8/CNT sample (Table S5), which may indicate Pd species act as a catalyst for N_8 decomposition. But 375 °C decomposition temperature is still promising for practical application.

Based on the structure illustrated in Fig. 3b, Pd sites on Pd_1-N_8/CNT are isolated as a result of the absence of neighboring Pd sites, which further leads to the effective reduction of the number of multiply coordinated sites of Pd (*i.e.*, geometric effect). The assumption is discreetly testified via C_2H_2-TPD by investigating the acetylene adsorption property over catalysts before and after CV treatment. The π-bonding system of acetylene can bond in two important configurations on the Pd surface, the weak π-bonding on a single Pd site (type I, *i.e.*, isolated sites) and the relatively strong σ-bonding to two or more neighboring sites (type II, *i.e.*, multiply coordinated sites) [46,47]. It was suggested that only type I adsorption can be hydrogenated in high selectivity to ethylene. In contrast, σ-bonded acetylene molecules lead to considerable formation of ethane by over-hydrogenation or green oil due to the decomposition of multiply bound C2 species and further polymerization on the catalyst under hydrogenation conditions [48]. These two types of adsorption can be identified by C_2H_2-TPD patterns via examining the desorption temperature. Figs. 4b and S5 presents the desorption signals for different samples. The obvious peaks were observed on all samples with three desorption temperature ranges. The peaks of 0 M and Pd/CNT (both without PN) appeared in Range 2 with temperature at around 200 °C, which was attributed to the superior activity of Pd. The desorption peak from PN/CNT (without Pd) is located in Range 3 at a temperature of around 400 °C. Due to the fact that the CNT showed no affinity to acetylene, this peak can be attributed to the existence of Lewis base PN species, which are active and can play the role as electron donors and tend to adsorb acetylene. The adsorbed acetylene was released as a result of PN decomposition at this range based on the above temperature-programmed decomposition results.

Interestingly, the samples containing both Pd and PN species (*i.e.*, Pd_1-N_8/CNT-0.5, 1, and 2 M) had two desorption peaks, one located in the lower temperature (Range 1, ~100 °C) while the other was at higher temperature (Range 3). The lower peaks originated from the weakly chemisorbed acetylene on Pd sites. The shift to lower temperature (200 → 100 °C) after CV treatment can be attributed to the electronic effect between PN and Pd as revealed in XPS analysis and Mulliken charge calculation (Fig. 3). The decreased electron density of Pd atom would weaken its adsorption intensity to acetylene and accordingly lower desorption temperature. Therefore, the introduction of N_8 into Pd/CNT makes it an "electronic additive" in the Pd_1-N_8/CNT catalysts, a common approach to improve the selectivity for acetylene hydrogenation in industry [29]. The higher desorption peaks also came from N_8 decomposition. To confirm the low temperature desorption of acetylene originating from the CV treatment, two reference samples, 0.01Pd-N_8/CNT and 0.01Pd/CNT, were prepared by wetness impregnation using N_8/CNT and CNT as support, respectively, while the Pd loading percentage was close to Pd_1-N_8/CNT-1 M sample(0.01% vs 0.0092%). Similar C_2H_2-TPD experiments over these two samples were carried out (Fig. S6). No low temperature desorption peak was observed, indicating that the CV process is crucial to the formation of configurations (*i.e.*, Pd_1-N_8 complex as shown in Fig. 3b) for the weak adsorption of acetylene.

Fig. 5 and Table S3 summarizes the results of selective hydrogenation of acetylene with different catalysts. Three reference catalysts showed different activities. Pd/CNT was very active for the

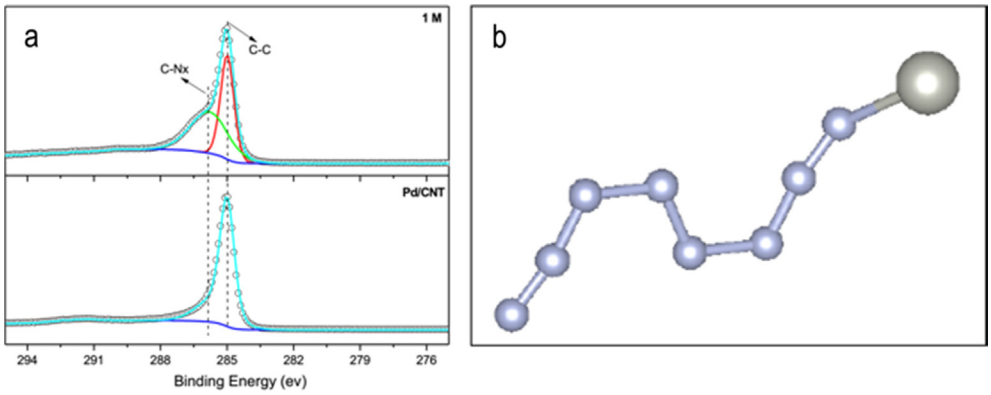

Fig. 3. C1s XPS spectra (a) of Pd_1-N_8/CNT-1 M and PdO/CNT; Small, open circles in black are the measured experiment points. The solid lines in cyan and blue are the sum of all the peak fittings and background, respectively. All the data analysis was accomplished using the commercial software Casa XPS, supplied by Casa Software Ltd; Interaction of Pd atom with PN within Pd_1-N_8 complex (b) using DFT calculations and Bader charge calculations.

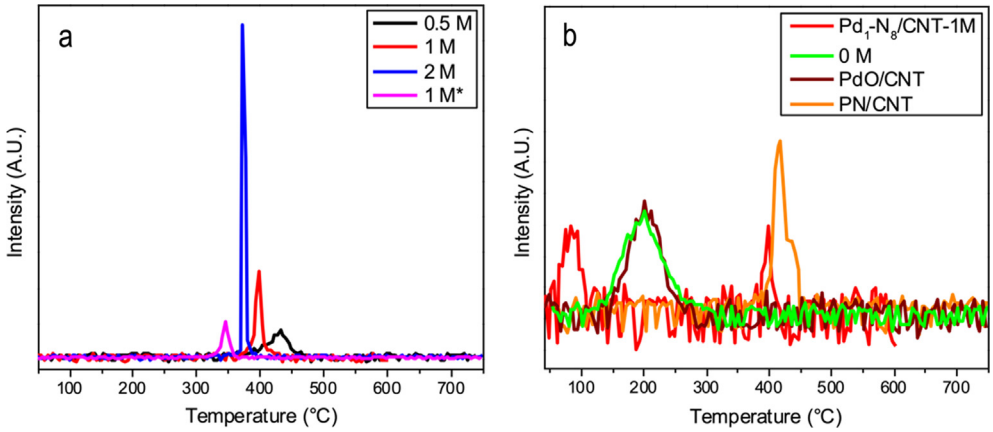

Fig. 4. (a) N^{14} signals normalized by sample weight from the temperature programmed decomposition results for dipped Pd/CNT and Pd_1-N_8/CNT sheets with different NaN_3 concentrations after CV synthesis; (b) MS signal (m/e = 26) for each C_2H_2-TPD measurement obtained from different catalysts where signals were normalized by samples weight.

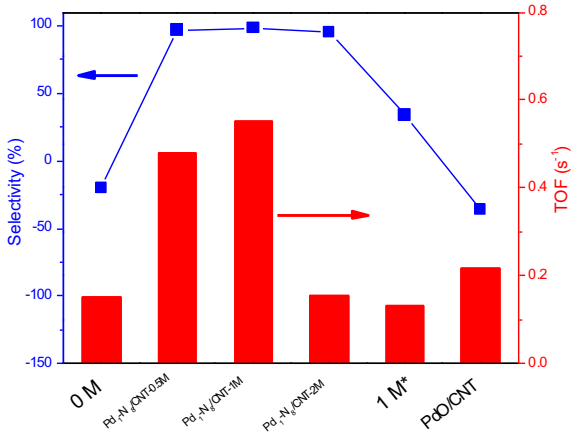

Fig. 5. TOF and ethylene selectivity during acetylene hydrogenation on different samples, measured by isothermal experiments at 40 °C.

hydrogenation reaction with 91.6% conversion, but negative selectivity for ethylene was achieved. A negative value indicated a net loss of ethylene due to the excessive hydrogenation of ethylene contained in the feed to produce ethane. Similar results were observed on 0 M except that the conversion was slightly lower than Pd/CNT. The positive selectivity value was collected on the third reference (1 M*) which may be attributed to the partial coverage of Pd by azide to promote the type I adsorption for acetylene. As expected, very high ethylene selectivity was obtained on samples with CV treatment in NaN_3 containing electrolyte. It could be attributed to single-atom Pd sites isolation, the electronic effect between Pd_1 and N_8, and a decrease of multiple sites. Isolation of single-atom Pd sites on the surface results in the absence of neighboring Pd sites, which would suppress the formation of di-σ-bonded alkene and alkyne species (type II adsorption) and lead to preferentially weakly π-bonded acetylene molecules on the catalyst surface (type I adsorption), thus promote the selectivity to ethylene. The decreased electron density of Pd_1 due to the presence of N_8 further weakens adsorption intensity to acetylene, providing extra force to improve the selectivity. Very limited conversions (0.1 and 1%, see Table S6) were achieved over 0.01Pd- N_8/CNT and 0.01Pd/CNT (both possess similar Pd loading with Pd_1-N_8/CNT-1 M), which are much lower than that of Pd_1-N_8/CNT-1 M (83.1%). Therefore, single atom Pd attached to N_8 (Fig. 3b) formed only during the CV is the active site for acetylene adsorption and selective hydrogenation. Turnover frequency (TOF) calculation results showed that Pd_1-N_8/CNT-1 M had the highest TOF (0.5528 s^{-1}) for selective hydrogenation of acetylene among all the samples, almost three times higher than that of pure Pd/CNT (0.217 s^{-1}). This confirms the Pd_1-N_8 (in Fig. 3b) is more active and selective to ethylene production.

To further confirm the experimental results, DFT was used to investigate this Pd_1-N_8/CNT system. The most energetically favor-

able attachment position of Pd was determined by placing a single Pd atom at numerous sites around the PN chain and performing full geometric optimizations and calculating the absorption energy (E_{ads}). The lowest adsorption energy occurred when the Pd atom adsorbed to the outermost N atom (Fig. 3b) with E_{ads} = −1.03 eV, indicating that adsorption of Pd is favorable on N_8 or N_8^-. The frequency calculation indicates that Pd_1-N_8 is more stable with a charge transfer of 0.23 *e* from the Pd atom to the N_8 chain, which is in agreement with experimental XPS measurements. When Pd_1-N_8 is attached to the inside or outside CNT surface, the calculation results show the CNT is necessary for the stabilization of the single atom Pd complex. Following a full relaxation of the Pd_1-N_8 system inside and outside a CNT (Fig. S7), a natural bond orbital calculation was performed. This showed that the complex has a charge of −0.50 *e* (when inside) and −0.15 *e* (when outside) net charge. The electric field generated by this negative complex and positive CNT is what stabilizes the Pd_1-N_8/CNT system [49].

To understand the improved C_2H_4 selectivity of the Pd_1-N_8/CNT system, the preferred C_2H_2 hydrogenation mechanism is explored. When C_2H_2, C_2H_3, C_2H_4, C_2H_5, or C_2H_6 molecules were placed in different positions on the Pd_1-N_8 complex, the most energetically favorable position from the full geometric relaxations in each case is when the molecule is adsorbed to the single Pd atom (Fig. S8). C_2H_2 and C_2H_4 bind in a π-bonded fashion in which the C—C bond is located on top of the single Pd atom (*i.e.*, the efficient type I adsorption configuration, Fig. S8a and c). E_{ads} for each species is negative (Table S11), indicting favorable adsorption. The DFT predicted stable chemisorption geometric structures are consistent with the experimental observations. It is well known that H_2 dissociates on metal sites on conventional supported metal catalysts including Pd/C. Interestingly, on the Pd_1-N_8/CNT system, the H_2 molecule adsorbs to the neighboring N atom (E_{ads} = −1.04 eV, Fig. S9a) instead of Pd_1; this configuration is significantly more favorable than co-adsorption of C_2H_2 and H_2 to the Pd atom by 1.05 eV. Moreover, H_2 adsorption is more favorable on N than Pd_1 (−0.98 eV versus −0.89 eV) in the absence of C_2H_2 on Pd. In both cases, the H_2 molecule dissociates to two adsorbed H atoms spontaneously (Fig. S9b). However, the adsorption of H_2 or an H atom leads to the further relaxation of the Pd_1-N_8 geometric structure; the chain spontaneously reorients such the Pd is bound to the first and fifth N atom, a configuration which allows for one of the adsorbed H atoms to migrate to the Pd atom through a transition state (TS 1, Fig. S8f) and form the C_2H_3 intermediate with a small energy barrier of 0.34 eV. The adsorption energy of C_2H_3 is much stronger than C_2H_2 ($E_{ads}[C_2H_2]$ = −1.37 eV, $E_{ads}[C_2H_3]$ = −2.56 eV), so the reaction continues to proceed. The second H atom migrates and forms C_2H_4 through TS 2 (Fig. S8g), with an energy barrier of 0.97 eV. At this point, the adsorption of C_2H_4 becomes less favorable than C_2H_2 ($E_{ads}[C_2H_2]$ = −1.04 eV, $E_{ads}[C_2H_4]$ = −0.91 eV]. Given this, it is therefore more favorable for C_2H_4 to desorb and a new C_2H_2 molecule to adsorb to the Pd site at this point, leading to the enhanced selection of ethylene by this Pd_1-N_8 system.

The hydrogenation of C_2H_4 to C_2H_6 was also investigated. The adsorption of another H_2 molecule to the Pd_1-N_8/C_2H_4 complex is again favorable, with an energy gain of −0.24 eV (Fig. S10a). However, even after H_2 adsorption it is still more favorable for C_2H_4 to desorb and C_2H_2 to adsorb (E_{ads} of −1.36 and −1.16 eV for C_2H_2 and C_2H_4 in the presence of H_2, respectively). Regardless, the migration of an H atom and subsequent formation of C_2H_5 would have to overcome an energy barrier of 0.95 eV through TS 3 (Fig. S8h). In addition to the preferred adsorption of C_2H_2 over C_2H_4, the fact that the desorption energy of C_2H_4 is lower than this TS 3 activation energy also leads to the observed C_2H_4 selectivity of this system. However, if the reaction continues to proceed, the second H atom goes through TS 4 (activation barrier of 0.98 eV) to form C_2H_6. As in other systems, C_2H_6 desorbs nearly spontaneously with $E_{ads}[C_2H_6]$ = −0.12 eV.

Moreover, a possible competing mechanism in which an H atom adsorbs to the Pd atom instead of the first N atom in the N_8 chain (Fig. S10b) was investigated. In this case the Pd_1-N_8 chain remains straight throughout the process, but the initial conversion to the C_2H_3 intermediate occurs through a transition state that is 1.36 eV higher than the starting adsorbed C_2H_2 reactant, making this first step significantly unfavorable when compared to the previously described mechanism, which further confirms the selective hydrogenation process occurs via H_2 and H atom adsorption to the neighboring N atom rather than the Pd single atom; the presence of the N_8 is therefore the reason for the improved C_2H_4 selectivity (Fig. 6).

This analysis reveals why selective hydrogenation of acetylene is better on the Pd_1-N_8 complex compared to a Pd(1 1 1) surface [50]. The activation barrier (TS 1) for the initial transformation of C_2H_2 to C_2H_3 is much lower on Pd_1-N_8 (0.34 eV) than Pd(1 1 1) (0.68 eV), while TS 2 and C_2H_4 desorption are roughly equivalent. Finally, the activation energy of TS 3, which prevents further hydrogenation of C_2H_4 to C_2H_5, is much higher on Pd_1-N_8 (0.95 eV) than on Pd(1 1 1) (0.75 eV). Moreover, Pd_1-N_8 preforms comparatively well with single atom Pd stabilized on other 2D materials, such as g-C_3N_4, albeit in a different manner [51]. Again, the initial conversion of C_2H_2 to C_2H_3 is lower on Pd_1-N_8 (0.34 eV) than g-C_3H_4 (0.93 eV). However, transformation of C2H to C_2H_4 is easier on g-C_3N_4 (0.26 versus 0.97 eV on Pd_1-N_8). Moreover, although it is easier for C_2H_4 to desorb from Pd_1-N_8 than g-C_3N_4 (Eads[C_2H_4] = 0.91 eV versus 1.02 eV, respectively), the TS 3 activation energy is higher on g-C_3N_4 (1.68 eV) than Pd_1-N_8 (0.95 eV).

A conventional isolation method like alloys reveals segregation of Pd to larger Pd ensembles with time on stream, resulting in limited selectivity and stability. In the present work, Pd_1-N_8/CNT-1 M was selected for the stability test. Fig. S11a shows that Pd_1-N_8/CNT-1 M exhibited long-term stability with a conversion of 83% and a selectivity of ~98% throughout 60 h on stream. To further investigate the stability of Pd_1-N_8/CNT-1 M sample, temperature-programmed oxidation (TPO) was carried out on a Pd_1-N_8/CNT-1 M catalyst after reaction and the data are shown in Fig. S11b. Fresh Pd_1-N_8/CNT-1 M catalyst was also tested with TPO as a reference under the same condition. A small amount of CO_2 was detected at low temperatures due to the adsorption of carbonaceous species over the catalyst [52–54]. The results illustrated that very little carbon species was deposited on the used samples. Therefore, no side reactions for oligomer formation or coke deposition occurred on Pd_1-N_8/CNT-1 M, which could explain its superior stability. HAADF-STEM images of used Pd_1-N_8/CNT-1 M (Fig. S12) also demonstrated clear single-atom structure, which further confirmed the high stability of Pd_1-N_8/CNT catalysts. Without CV treatment, acetylene is adsorbed mostly on multiple sites, which results into poor selectivity to ethylene as well as the mass production of ethane and green oil. With CV treatment, Pd ensembles are eliminated, which leads to isolated single-atom sites dominating on the surface and further promotes selectivity to desired ethylene as well as suppresses the side reactions.

4. Conclusion

In conclusion, distinct from conventional annealing methods to establish covalent interactions between metals or making alloys with harsh condition, we have presented a facile electrochemical treatment method to synthesize an isolated single-atom catalyst with high performance for selective hydrogenation of acetylene under ambient condition. Single atom Pd attached to a designed

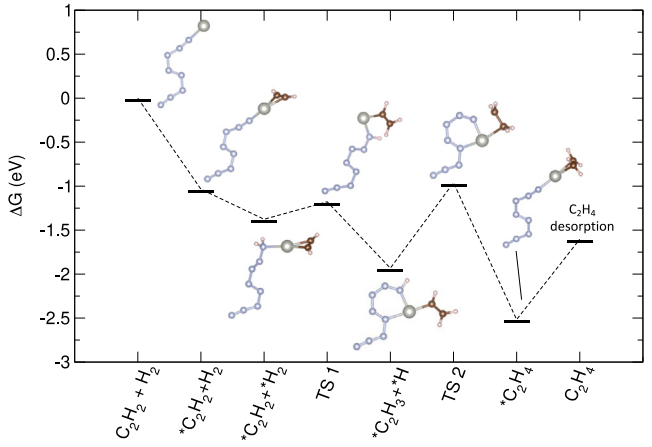

Fig. 6. Reaction free energy diagram of selective hydrogenation of C_2H_2 to C_2H_4 by Pd_1-N_8.

Lewis base N_8 on CNT substrate (Pd_1-N_8/CNT) was successfully synthesized with the CV method. Both experimental and DFT theoretical work confirmed that Pd_1-N_8 was more active and selective towards ethylene production. Different from the conventional metal catalysts that H_2 dissociated on metal site, here H_2 dissociated on N site. Moreover, the charge transfer between Pd and N_8 prevented Pd agglomeration, made Pd_1-N_8/CNT superior to the conventional systems. Thus the optimized Pd_1-N_8/CNT exhibited long term stability with a conversion of 83%, an ethylene selectivity of ~98%.

Declaration of Competing Interest

The authors declare that they have no known competing financial interests or personal relationships that could have appeared to influence the work reported in this paper.

Acknowledgements

This work was supported by an ACS-PRF 53582-ND10 and partially NSF CBET-1804949. C. Wang thanks the support of PNNL LDRD. The microscopic and XPS analysis in this work was conducted in the William R. Wiley Environmental Molecular Sciences Laboratory (EMSL), a national scientific user facility sponsored by DOE's Office of Biological and Environmental Research and located at PNNL. PNNL is operated by Battelle for the Department of Energy under Contract DE-AC05-76RLO1830. M. Hu thanks the support from Science and Technology Research Project of Education Department of Hubei Province (B2020229). DFT calculations were performed using the Kong and Lochness High Performance Computing clusters at the New Jersey Institute of Technology.

Appendix A. Supplementary material

Supplementary data to this article can be found online at https://doi.org/10.1016/j.jcat.2020.12.009.

References

[1] X. Huang, H. Yan, L. Huang, X. Zhang, Y. Lin, J. Li, Y. Xia, Y. Ma, Z. Sun, S. Wei, J. Lu, Toward understanding of the support effect on Pd_1 single-atom-catalyzed hydrogenation reactions, J. Phys. Chem. C 123 (2019) 7922–7930.
[2] A. Wang, J. Li, T. Zhang, Heterogeneous single-atom catalysis, Nat. Rev. Chem. 2 (2018) 65–81.
[3] X. Li, Y. Huang, B. Liu, Catalyst: single-atom catalysis: directing the way toward the nature of catalysis, Chem 5 (2019) 2733–2735.
[4] M. Hu, X. Wang, Effect of N_3^- species on selective acetylene hydrogenation over Pd/SAC catalysts, Catal. Today 263 (2016) 98–104.
[5] C.W. Chan, A.H. Mahadi, M.M. Li, E.C. Corbos, C. Tang, G. Jones, W.C. Kuo, J. Cookson, C.M. Brown, P.T. Bishop, S.C. Tsang, Interstitial modification of palladium nanoparticles with boron atoms as a green catalyst for selective hydrogenation, Nat. Commun. 5 (2014) 5787.
[6] W.-J. Kim, S.H. Moon, Modified Pd catalysts for the selective hydrogenation of acetylene, Catal. Today 185 (2012) 2–16.
[7] G. Vilé, P. Dähler, J. Vecchietti, M. Baltanás, S. Collins, M. Calatayud, A. Bonivardi, J. Pérez-Ramírez, Promoted ceria catalysts for alkyne semi-hydrogenation, J. Catal. 324 (2015) 69–78.
[8] W.G. Menezes, L. Altmann, V. Zielasek, K. Thiel, M. Bäumer, Bimetallic Co-Pd catalysts: study of preparation methods and their influence on the selective hydrogenation of acetylene, J. Catal. 300 (2013) 125–135.
[9] M. Armbrüster, R. Schlögl, Y. Grin, Intermetallic compounds in heterogeneous catalysis - a quickly developing field, Sci. Tech. Adv. Mater. 15 (2014).
[10] C. Ma, Y. Du, J. Feng, X. Cao, J. Yang, D. Li, Fabrication of supported PdAu nanoflower catalyst for partial hydrogenation of acetylene, J. Catal. 317 (2014) 263–271.
[11] J.A. Bennett, G.A. Attard, K. Deplanche, M. Casadesus, S.E. Huxter, L.E. Macaskie, J. Wood, Improving selectivity in 2-butyne-1,4-diol hydrogenation using biogenic Pt catalysts, ACS Catal. 2 (2012) 504–511.
[12] J. Prinz, C.A. Pignedoli, Q.S. Stockl, M. Armbruster, H. Brune, O. Groning, R. Widmer, D. Passerone, Adsorption of small hydrocarbons on the three-fold PdGa surfaces: the road to selective hydrogenation, J. Am. Chem. Soc. 136 (2014) 11792–11798.
[13] A. Borodziński, G.C. Bond, Selective hydrogenation of ethyne in ethene-rich streams on palladium catalysts. Part 1. Effect of changes to the catalyst during reaction, Cat. Rev. - Sci. Eng. 48 (2006) 91–144.
[14] M. Armbrüster, M. Behrens, F. Cinquini, K. Föttinger, Y. Grin, A. Haghofer, B. Klötzer, A. Knop-Gericke, H. Lorenz, A. Ota, S. Penner, J. Prinz, C. Rameshan, Z. Révay, D. Rosenthal, G. Rupprechter, P. Sautet, R. Schlögl, L. Shao, L. Szentmiklósi, D. Teschner, D. Torres, R. Wagner, R. Widmer, G. Wowsnick, How to control the selectivity of palladium-based catalysts in hydrogenation reactions: the role of subsurface chemistry, ChemCatChem 4 (2012) 1048–1063.
[15] A. Borodziński, G.C. Bond, Selective hydrogenation of ethyne in ethene-rich streams on palladium catalysts, Part 2: Steady-state kinetics and effects of palladium particle size, carbon monoxide, and promoters, Cat. Rev. - Sci. Eng. 50 (2008) 379–469.
[16] J. Osswald, K. Kovnir, M. Armbrüster, R. Giedigkeit, R.E. Jentoft, U. Wild, Y. Grin, R. Schlögl, Palladium–gallium intermetallic compounds for the selective hydrogenation of acetylene: Part II: Surface characterization and catalytic performance, J. Catal. 258 (2008) 219–227.
[17] B. Qiao, A. Wang, X. Yang, L.F. Allard, Z. Jiang, Y. Cui, J. Liu, J. Li, T. Zhang, Single-atom catalysis of CO oxidation using Pt_1/FeO_x, Nat. Chem. 3 (2011) 634–641.
[18] G.X. Pei, X.Y. Liu, A. Wang, A.F. Lee, M.A. Isaacs, L. Li, X. Pan, X. Yang, X. Wang, Z. Tai, K. Wilson, T. Zhang, Ag alloyed Pd single-atom catalysts for efficient selective hydrogenation of acetylene to ethylene in excess ethylene, ACS Catal. 5 (2015) 3717–3725.
[19] J. Liu, F.R. Lucci, M. Yang, S. Lee, M.D. Marcinkowski, A.J. Therrien, C.T. Williams, E.C.H. Sykes, M. Flytzani-Stephanopoulos, Tackling CO poisoning with single-atom alloy catalysts, J. Am. Chem. Soc. 138 (2016) 6396–6399.
[20] Q. Feng, S. Zhao, Y. Wang, J. Dong, W. Chen, D. He, D. Wang, J. Yang, Y. Zhu, H. Zhu, Isolated single-atom Pd sites in intermetallic nanostructures: high catalytic selectivity for semihydrogenation of alkynes, J. Am. Chem. Soc. 139 (2017) 7294–7301.
[21] S. Zhou, L. Shang, Y. Zhao, R. Shi, G.I.N. Waterhouse, Y.-C. Huang, L. Zheng, T. Zhang, Pd single-atom catalysts on nitrogen-doped graphene for the highly selective photothermal hydrogenation of acetylene to ethylene, Adv. Mater. 31 (2019) 1900509.
[22] S. Liang, C. Hao, Y. Shi, The power of single-atom catalysis, ChemCatChem 7 (2015) 2559–2567.
[23] C. Zhu, S. Fu, Q. Shi, D. Du, Y. Lin, Single-atom electrocatalysts, Angew. Chem. Int. Ed. 56 (2017) 13944–13960.
[24] H. Wang, J. Dong, L.F. Allard, S. Lee, S. Oh, J. Wang, W. Li, M. Shen, M. Yang, Single-site $Pt/La-Al_2O_3$ stabilized by barium as an active and stable catalyst in purifying CO and C_3H_6 emissions, Appl. Catal., B 244 (2019) 327–339.
[25] R.E. McGovern, S.C. Feifel, F. Lisdat, P.B. Crowley, Microscale crystals of cytochrome c and calixarene on electrodes: interprotein electron transfer between defined sites, Angew. Chem. Int. Ed. 54 (2015) 6356–6359.
[26] M. Tavakkoli, N. Holmberg, R. Kronberg, H. Jiang, J. Sainio, E.I. Kauppinen, T. Kallio, K. Laasonen, Electrochemical activation of single-walled carbon nanotubes with pseudo-atomic-scale platinum for the hydrogen evolution reaction, ACS Catal. 7 (2017) 3121–3130.
[27] L. Zhang, L. Han, H. Liu, X. Liu, J. Luo, Potential-cycling synthesis of single platinum atoms for efficient hydrogen evolution in neutral media, Angew. Chem. Int. Ed. 56 (2017) 13694–13698.
[28] Z. Wu, E.M. Benchafia, Z. Iqbal, X. Wang, N_8 polynitrogen stabilized on multi-wall carbon nanotubes for oxygen-reduction reactions at ambient conditions, Angew. Chem. Int. Ed. 53 (2014) 12555–12559.
[29] D.C. Huang, K.H. Chang, W.F. Pong, P.K. Tseng, K.J. Hung, W.F. Huang, Effect of Ag-promotion on Pd catalysts by XANES, Catal. Lett. 53 (1998) 155–159.
[30] L. Shao, W. Zhang, M. Armbrüster, D. Teschner, F. Girgsdies, B. Zhang, O. Timpe, M. Friedrich, R. Schlögl, D. Su, Nanosizing intermetallic compounds onto carbon nanotubes: active and selective hydrogenation catalysts, Angew. Chem. Int. Ed. 50 (2011) 10231–10235.

[31] F. Neese, The ORCA program system, WIREs computational molecular, Science 2 (2012) 73–78.
[32] C. Lee, W. Yang, R.G. Parr, Development of the Colle-Salvetti correlation-energy formula into a functional of the electron density, Phys. Rev. B 37 (1988) 785–789.
[33] R.S. Mulliken, Electronic population analysis on LCAO–MO molecular wave functions. I, J. Chem. Phys. 23 (1955) 1833–1840.
[34] Y. He, L. Liang, Y. Liu, J. Feng, C. Ma, D. Li, Partial hydrogenation of acetylene using highly stable dispersed bimetallic Pd–Ga/MgO–Al_2O_3 catalyst, J. Catal. 309 (2014) 166–173.
[35] Q. Guan, C. Yang, S. Wang, L. He, Z. Kong, X. Chai, H. Xin, P. Ning, Reactive metal-biopolymer interactions for semihydrogenation of acetylene, ACS Catal. 9 (2019) 11146–11152.
[36] E.A. Monyoncho, S. Ntais, F. Soares, T.K. Woo, E.A. Baranova, Synergetic effect of palladium-ruthenium nanostructures for ethanol electrooxidation in alkaline media, J. Power Sources 287 (2015) 139–149.
[37] F.D. Sypaseuth, C. Matlachowski, M. Weber, M. Schwalbe, C.C. Tzschucke, Electrocatalytic carbon dioxide reduction by using cationic pentamethylcyclopentadienyl-iridium complexes with unsymmetrically substituted bipyridine ligands, Chem. Eur. J. 21 (2015) 6564–6571.
[38] A.V. Ananiev, V.P. Shilov, P. Brossard, Kinetics of the platinum catalyzed hydrazoic acid decomposition in acidic media, Appl. Catal., A 257 (2004) 151–156.
[39] M. Li, Q. Sun, C.-J. Liu, Preparation of floating Au/PVP film on water for a green and rapid extraction of gold ion, ACS Sustainable Chem. Eng. 4 (2016) 3255–3260.
[40] J. Ji, J. Wen, Y. Shen, Y. Lv, Y. Chen, S. Liu, H. Ma, Y. Zhang, Simultaneous noncovalent modification and exfoliation of 2D carbon nitride for enhanced electrochemiluminescent biosensing, J. Am. Chem. Soc. 139 (2017) 11698–11701.
[41] H. Abou-Rachid, A. Hu, V. Timoshevskii, Y. Song, L.-S. Lussier, Nanoscale high energetic materials: a polymeric nitrogen chain confined inside a carbon nanotube, Phys. Rev. Lett. 100 (2008) 196401.
[42] Z. Chen, S. Mitchell, E. Vorobyeva, R.K. Leary, R. Hauert, T. Furnival, Q.M. Ramasse, J.M. Thomas, P.A. Midgley, D. Dontsova, M. Antonietti, S. Pogodin, N. López, J. Pérez-Ramírez, Stabilization of single metal atoms on graphitic carbon nitride, Adv. Funct. Mater. 27 (2017) 1605785.
[43] W. Zhang, H. Huang, F. Li, K. Deng, X. Wang, Palladium nanoparticles supported on graphitic carbon nitride-modified reduced graphene oxide as highly efficient catalysts for formic acid and methanol electrooxidation, J. Mater. Chem. A 2 (2014) 19084–19094.
[44] Q. Wang, J. Che, Origins of distinctly different behaviors of Pd and Pt contacts on graphene, Phys. Rev. Lett. 103 (2009) 066802.
[45] K.M. Deyle, B. Farrow, Y. Qiao Hee, J. Work, M. Wong, B. Lai, A. Umeda, S.W. Millward, A. Nag, S. Das, J.R. Heath, A protein-targeting strategy used to develop a selective inhibitor of the E17K point mutation in the PH domain of Akt1, Nat. Chem. 7 (2015) 455–462.
[46] J. Osswald, K. Kovnir, M. Armbruster, R. Giedigkeit, R. Jentoft, U. Wild, Y. Grin, R. Schlogl, Palladium–gallium intermetallic compounds for the selective hydrogenation of acetylenePart II: Surface characterization and catalytic performance, J. Catal. 258 (2008) 219–227.
[47] S.K. Kim, C. Kim, J.H. Lee, J. Kim, H. Lee, S.H. Moon, Performance of shape-controlled Pd nanoparticles in the selective hydrogenation of acetylene, J. Catal. 306 (2013) 146–154.
[48] A. Doyle, Alkene chemistry on the palladium surface: nanoparticles vs single crystals, J. Catal. 223 (2004) 444–453.
[49] W. Ji, V. Timoshevskii, H. Guo, H. Abou-Rachid, L.-S. Lussier, Thermal stability and formation barrier of a high-energetic material N_8 polymer nitrogen encapsulated in (5,5) carbon nanotube, Appl. Phys. Lett. 95 (2009) 021904.
[50] P.A. Sheth, M. Neurock, C.M. Smith, A first-principles analysis of acetylene hydrogenation over Pd(111), J. Phys. Chem. B 107 (2003) 2009–2017.
[51] Y. Zhao, M. Zhu, L. Kang, The DFT study of single-atom Pd_1/g-C_3N_4 catalyst for selective acetylene hydrogenation reaction, Catal. Lett. 148 (2018) 2992–3002.
[52] H. Bazzazzadegan, M. Kazemeini, A.M. Rashidi, A high performance multi-walled carbon nanotube-supported palladium catalyst in selective hydrogenation of acetylene-ethylene mixtures, Appl. Catal., A 399 (2011) 184–190.
[53] J. Ashok, S. Kawi, Nickel-iron alloy supported over iron-alumina catalysts for steam reforming of biomass tar model compound, ACS Catal. 4 (2014) 289–301.
[54] N. Tsubouchi, Y. Ohtsuka, H. Hashimoto, T. Yamada, H. Hashimoto, Chemical characterization of unburned carbon in coal fly ashes by use of TPD/TPO and LRS methods, Environ. Sci. Technol. 49 (2015) 5189–5194.